

# ISVR Technical Memorandum

## SCIENTIFIC PUBLICATIONS BY THE ISVR

*Technical Reports* are published to promote timely dissemination of research results by ISVR personnel. This medium permits more detailed presentation than is usually acceptable for scientific journals. Responsibility for both the content and any opinions expressed rests entirely with the author(s).

*Technical Memoranda* are produced to enable the early or preliminary release of information by ISVR personnel where such release is deemed to be appropriate. Information contained in these memoranda may be incomplete, or form part of a continuing programme; this should be borne in mind when using or quoting from these documents.

*Contract Reports* are produced to record the results of scientific work carried out for sponsors, under contract. The ISVR treats these reports as confidential to sponsors and does not make them available for general circulation. Individual sponsors may, however, authorize subsequent release of the material.

### COPYRIGHT NOTICE

(c) ISVR University of Southampton All rights reserved.

ISVR authorises you to view and download the Materials at this Web site ("Site") only for your personal, non-commercial use. This authorization is not a transfer of title in the Materials and copies of the Materials and is subject to the following restrictions: 1) you must retain, on all copies of the Materials downloaded, all copyright and other proprietary notices contained in the Materials; 2) you may not modify the Materials in any way or reproduce or publicly display, perform, or distribute or otherwise use them for any public or commercial purpose; and 3) you must not transfer the Materials to any other person unless you give them notice of, and they agree to accept, the obligations arising under these terms and conditions of use. You agree to abide by all additional restrictions displayed on the Site as it may be updated from time to time. This Site, including all Materials, is protected by worldwide copyright laws and treaty provisions. You agree to comply with all copyright laws worldwide in your use of this Site and to prevent any unauthorised copying of the Materials.

UNIVERSITY OF SOUTHAMPTON  
INSTITUTE OF SOUND AND VIBRATION RESEARCH  
DYNAMICS GROUP

**Nonlinear Shaping of a Spectral Excitation Matrix for a Linear Road/Tyre  
Interaction Stochastic Analysis**

by

**E. Rustighi and S.J. Elliott**

ISVR Technical Memorandum No: 985

March 2009

Authorised for issue by  
Professor M. J. Brennan  
Group Chairman

## Contents

<b>Abstract</b>	<b>iv</b>
<b>1 Introduction</b>	<b>1</b>
<b>2 The linear tyre excitation matrix</b>	<b>1</b>
2.1 The power spectrum of the road profile . . . . .	2
2.2 The excitation matrix . . . . .	3
<b>3 The nonlinear tyre excitation matrix</b>	<b>3</b>
3.1 The road profile . . . . .	4
3.2 The nonlinear excitation matrix . . . . .	4
<b>4 Approximated tyre excitation matrix</b>	<b>7</b>
<b>5 Validation on a 2D linear model</b>	<b>8</b>
<b>6 Conclusions</b>	<b>9</b>
<b>7 Figures</b>	<b>11</b>
<b>References</b>	<b>21</b>

## List of Figures

1	Piecewise linear approximation of the PSD of a common road profile and PSD of the generated road profile used in the time-domain nonlinear simulations . . . . .	11
2	Representation across the contact patch of $\mathbf{R}^{\text{lin}}$ . . . . .	12
3	Schematic representation of the nonlinear contact algorithm. . .	13
4	Road profile before and after the application of the nonlinear transformation . . . . .	14
5	Spectra of the nonlinear excitation spectral matrix and coherences between the nonlinear contact displacements . . . . .	15
6	Representation across the contact patch of $\mathbf{R}^{\text{nl}}$ . . . . .	16
7	Change of the mean value of the diagonal of the matrix $\mathbf{R}^{\text{nl}}$ with the bedding stiffness for various road profiles rms . . . . .	17
8	Variation of fitted value of the parameter $c_f$ with the road roughness . . . . .	18
9	Average kinetic energy spectrum and rms velocity around the tyre . . . . .	19

## Abstract

Tyre/road interaction is recognised as the main source of interior and exterior noise in vehicles at velocities over 40 km/h. Previously, the authors proposed a linear stochastic approach to predict the tyre vibrations due to the road/tyre interaction. A mechanical model of the tyre was connected to the road through a series of parallel springs (Winkler model) assumed to be in contact with the road at all the time. Such a linear model is only strictly valid for smooth road and soft tyres. In this paper, the range of validity of the linearity assumption is investigated and, a modified shape of the excitation matrix, that takes into account the contact nonlinearity, is proposed. The investigation is based on a 2D numerical nonlinear model of the tyre/road contact so that the displacements of the contact springs can be used to evaluate the nonlinear excitation matrix. An approximated nonlinear excitation spectrum has been proposed and his validity has been checked on a 2D linear tyre model.

## 1 Introduction

Sandberg and Descornet [1] provided strong arguments that the low frequency car exterior noise, below 800 Hz, is related to the tyre vibrations. However, these authors could not find a linear relationship between the macrotexture of the road and the external noise, which is thought to be because of the nonlinearity between sound and profile amplitudes. Fong [2] investigated the contact pressure induced by the road macrotexture (irregularities sized from 0.5 to 50 mm) to predict near field tyre noise. He showed that the transfer function between contact pressure, computed by a half-space approximation, and the near-field tyre noise are not linearly correlated with the road texture. This suggests that the nonlinearity due to the contact between the asphalt and the tyre is the main reason for the poor correlation between the road profile and the interior or exterior car noise.

Rustighi and Elliott [3] proposed a two-dimensional linear model to predict the random excitation of a tyre's vibration due to the tyre/road interaction in the frequency range up to 400 Hz, where the dominant vibration is two-dimensional. The tyre was modelled as an elemental system, which permitted the analysis of the low frequency tyre response when excited by distributed stochastic displacements in the contact patch. A linear model was used to calculate the contact forces from the road roughness and thus calculate the average spectral properties of the resulting radial velocity of the tyre in one step from the spectral properties of the road roughness. The linear contact model assumes that the tyre is smooth and soft enough that the whole of the tyre surface in the contact patch connects with the road. The analysis was entirely linear in order to exploit the simple theoretical formulation of a stochastic linear analysis and to develop a method that is computationally efficient. Even if the tyre model can be improved and made more detailed, the linearity in the contact model remains the main limiting assumption.

In this paper the authors investigate the possibility of extending the approach described in [3] to representing nonlinear situations, by means of a reshaping of the linear spectral excitation matrix. In this paper linear and nonlinear spectral excitation matrices are computed and compared. An approximated nonlinear excitation matrix based on fitting the root mean square (rms) values of the nonlinear excitation matrix is then proposed. The effectiveness of the approximation has been checked on the 2D tyre model and compared to the results from linear and nonlinear simulations.

## 2 The linear tyre excitation matrix

The excitation of a tyre due to its interaction with the road, under linearity assumptions, can be found by simple matrix multiplications [3]. A Winkler model [4] can be used to model the interaction between tyre and road. The tyre

is connected to the ground at  $N_c$  points, at which the excitation is transmitted from the road to the tyre through a set of linear, uncoupled, parallel springs. The linearity assumption implies that all contact springs touch the road at all times. In this case, the spectral excitation matrix is related to the road profile and can be straightforwardly computed.

## 2.1 The power spectrum of the road profile

The road profile is usually assumed to be a random stationary process, hence it can be described in the wavelength domain by its power spectral density (PSD)  $G(n)$  [5], where  $n$  is the wavenumber expressed in cycles/m. A common description of the road profile, adopted for instance by Dodds and Robson [6], describe  $G(n)$  as Brownian noise,  $G(n) = C_0 n^{-2}$ . Such description is very simple but limited to wavelength between 1 and 100 m. Such wavelength range is not appropriate to study contact problem, where the common contact patch length  $L_c$  is usually 10 cm. When the wavelength range has to be extended  $G(n)$  can be expressed, for example, as  $G(n) = C_1 n^{-4} + C_2 n^{-2} + C_3$ , as suggested by Sayers [7]. A similar spectral distribution to that proposed by Sayers can be obtained with a piecewise linear approximation. In particular the following piecewise linear function has been chosen:

$$G_{rr}(n) = \begin{cases} cn^{-2} & \text{for } n_1 \leq n < n_2 \\ cn_2^{-2} & \text{for } n_2 \leq n \leq n_3 \\ c \left(\frac{n_2}{n_3}\right)^{-2} n^{-2} & \text{for } n_3 < n \leq n_4 \\ 0 & \text{for } n > n_4; n < n_1 \end{cases} \quad (1)$$

where  $c$  is a constant that in the frequency range above 1 m wavelength has the value suggested in [8], and  $n_1, n_2, n_3$  and  $n_4$  are constants that define the frequency range. They have been chosen as:  $n_1 = 1$  cycles/m,  $n_2 = 10$  cycles/m,  $n_3 = 200$  cycles/m and  $n_4 = 1000$  cycles/m. Fig. 1 shows the resulting PSD of the road profile. The first wavenumber range ( $n_1 \leq n < n_2$ ) has the characteristics of Brownian noise as described by [6]. The curve then assumes the characteristic of white noise in the second frequency range ( $n_2 \leq n \leq n_3$ ) as described by Sayers [7]. The third frequency range ( $n_3 < n \leq n_4$ ) has again the characteristic of Brownian noise.

The road profile of Eq. (1) has been normalised with respect to its rms value,  $x_{\text{rms}}^r$ , to define the constant  $c$ . The square of the rms value,  $(x_{\text{rms}}^r)^2$ , can be found by integration of Eq. (1)

$$(x_{\text{rms}}^r)^2 = \int_0^\infty G_{rr}(n) dn = c \left[ \frac{n_3 - n_2}{n_2^2} - \frac{1}{n_2} + \frac{1}{n_1} + \left(\frac{n_2}{n_3}\right)^{-2} \left(\frac{1}{n_3} - \frac{1}{n_4}\right) \right] \quad (2)$$

or by its definition as the average of the signal square.

## 2.2 The excitation matrix

In a linear contact model, the contact springs follow the road displacement at all times and the linear excitation matrix  $\mathbf{S}_{dd}^{\text{lin}}$  may be found from the road profile PSD by taking into account the time delay that there is in the excitation between different springs. The PSD of the road in the time domain can be found from Eq. (1) considering that the road is moving at velocity  $v$  [9]. Hence, the linear spectral density matrix  $\mathbf{S}_{dd}^{\text{lin}}$  is given by

$$\mathbf{S}_{dd}^{\text{lin}}(\omega) = \begin{bmatrix} S_{rr}(\omega) & S_{rr}(\omega) e^{j\omega \frac{\Delta x_{12}}{v}} & S_{rr}(\omega) e^{j\omega \frac{\Delta x_{13}}{v}} & \dots \\ S_{rr}(\omega) e^{-j\omega \frac{\Delta x_{12}}{v}} & S_{rr}(\omega) & S_{rr}(\omega) e^{j\omega \frac{\Delta x_{23}}{v}} & \dots \\ S_{rr}(\omega) e^{-j\omega \frac{\Delta x_{13}}{v}} & S_{rr}(\omega) e^{-j\omega \frac{\Delta x_{23}}{v}} & S_{rr}(\omega) & \dots \\ \vdots & \vdots & \vdots & \ddots \end{bmatrix} \quad (3)$$

where  $S_{rr}(\omega)$  is the frequency-domain version of the PSD of Eq. (1), obtained by letting  $\omega = 2\pi nv$ , where  $v$  is the vehicle velocity. It is noteworthy that the integral over frequency of the absolute value of each element of  $\mathbf{S}_{dd}^{\text{lin}}$  is equal to the rms value of the road profile  $x_{\text{rms}}^r$ . The result is obvious for the element along the diagonal since these are the power spectra of the road profile. The matrix  $\mathbf{R}^{\text{lin}}$ , that contains such integrals, called here the linear rms excitation matrix, is then given by

$$\mathbf{R}^{\text{lin}} = \sqrt{\int_0^\infty |\mathbf{S}_{dd}^{\text{lin}}(\omega)| d\omega} = x_{\text{rms}}^r \mathbf{U} \quad (4)$$

where  $\mathbf{U}$  is the unitary matrix, containing one in all elements. Fig. 2(a) shows the element of the matrix  $\mathbf{R}^{\text{lin}}$  for a road of roughness  $x_{\text{rms}}^r=2.5$  mm. The linear rms excitation matrix is evidently constant along the contact patch, as expected. Fig. 2(b) shows the time delay of each element of the matrix  $\mathbf{S}_{dd}^{\text{lin}}$  of Eq. (3). Since the distance between the contact point is growing linearly, the time delay grows accordingly.

## 3 The nonlinear tyre excitation matrix

The contact between tyre and road is usually nonlinear since the tyre contact points do not touch the road at all times. Since the system is time varying, a quasi static time domain approach has been used to solve the problem. The tyre has been modelled with a rigid flat surface that is pressed against the road through an array of springs in parallel (Winkler model). The length of the contact patch has been fixed to 10 cm [10]. The curvature of the tyre has not been taken into account since it has been supposed that the curvature is only related to the tyre deformation and not to the local contact deformation. The linear springs, distributed with the same spacing as the road description,

all have the same stiffness. When the tyre is pressed against the bedding the equilibrium point is iteratively solved using an algorithm that calculates how many springs are in contact and if their compression is enough to balance the force applied to the tyre, which is assumed constant. Although the dynamics of the vehicle could be taken into account to derive a time-varying balancing force, this variation is only expected to be significant at comparatively low frequencies and has not been incorporated here.

Fig. 3 shows the contact model and the quantities involved in the algorithm. The inputs of the algorithm are the road profile,  $x^r$ , and the force applied to the tyre,  $F^t$ , while the outputs are the displacement of the  $N_c$  contact springs,  $x_i^s$  ( $i = 1, \dots, N_c$ ), and the tyre displacement,  $x^t$ . The force applied to the tyre has been set as the weight of a quarter of an average car (2500 N).

### 3.1 The road profile

The road profile has been obtained from the piecewise linear PSD of the road profile in Eq. (1). From this PSD it is possible to calculate an example of a road profile in the spatial domain, by applying the inverse Fourier transform to the magnitude of the PSD and assuming a random, uniformly distributed phase. As a consequence of the central limit theorem, the road profile will then have a normal distribution. Unfortunately, this is not realistic and most roads do not have very high peaks, since they are usually rolled out [11, 12]. A nonlinear transformation has thus been adopted to remove these peaks. Fig. 4 shows the road profile before and after the application of this transformation. The red dotted line shows the road profile before applying the transformation, which has got a normal distribution. The continuous blue line shows the road profile after the transformation has been applied. This profile,  $x^r$ , is used in the nonlinear contact computation. The calculated PSD for this profile is still a good estimation of the piecewise linear road characteristic, as shown in Fig. 1, where the blue line is the PSD of  $x^r$ . The average level of the PSD has fallen by about 3 dB from the original Gaussian profile due to the removal of the peaks.

### 3.2 The nonlinear excitation matrix

As illustrated in Fig. 3, the Winkler nonlinear contact model provides the displacement of each spring,  $x_i^s$ , and that of the tyre,  $x^t$ , for a given road profile,  $x^r$ , and a given contact stiffness  $k_w$ . From now on, a frequency-domain formulation will be used so that each displacement variable corresponds to the Fourier transform of a long time history, although the explicit dependence on frequency,  $\omega$ , will be suppressed for notational convenience. The individual complex spring displacement spectra are grouped together in a vector,  $\mathbf{d}$ , equal to  $\{x_1^s, \dots, x_{N_c}^s\}^T$ , and the spectral density matrix of the excitation

displacements is then defined to be

$$\mathbf{S}_{dd}^{\text{nl}} = \text{E}[\mathbf{d}\mathbf{d}^{\text{H}}] \quad (5)$$

where E denotes the expectation operator and the superscript <sup>H</sup> denotes the Hermitian, complex conjugate, transpose. The diagonal elements of  $\mathbf{S}_{dd}^{\text{nl}}$  correspond to the power spectral densities of each of the displacements and the off-diagonal terms correspond to cross spectral densities between the displacements at different points.

Fig. 5(a) shows three auto-spectra of the nonlinear excitation spectral matrix (diagonal element of  $\mathbf{S}_{dd}^{\text{nl}}$ ) calculated from the nonlinear simulation with  $x_{\text{rms}}^r=2.5$  mm and  $k_w=180$  kN/m. The continuous blue line refers to a point at the edge of the contact patch, the dot-dash red line to the point in the centre of the contact patch and the dashed green line to the point between these two. The three lines overlap, showing that the nonlinearity does not affect the magnitudes of the diagonal elements of the excitation matrix. The shapes of the magnitudes of the cross spectral densities on the off-diagonal terms in  $\mathbf{S}_{dd}^{\text{nl}}$  are also relatively unchanged from the linear cases. Fig. 5(b) shows the coherences between the nonlinear contact displacements of different springs, again for ( $x_{\text{rms}}^r=2.5$  mm and  $k_w=180$  kN/m). The continuous blue line represents the coherence between two points 23 mm apart, the dashed green line to points 47 mm apart and the dot-dash red line to points 70 mm apart. Increasing the distance between the contact points thus decreases the correlation between the forces on the tyre.

From the nonlinear excitation matrix,  $\mathbf{S}_{dd}^{\text{nl}}$ , the square root of the integral over frequency of the absolute value of each element can be evaluated, and it is possible to calculate the matrix  $\mathbf{R}^{\text{nl}}$ , which is called here the nonlinear rms excitation matrix, and is defined by analogy with  $\mathbf{R}^{\text{lin}}$  in Eq. (4). The diagonal elements of the matrix are the rms value of the individual spring deformations, while the off-diagonal term are the square root of the correlation between the two deformations delayed in time by the distance between the two contact points. Hence, the diagonal elements of such matrix give information on the contact time of each spring and the off-diagonal terms are indicators of the correlation between different displacements.

Fig. 6(a) shows  $\mathbf{R}^{\text{nl}}$  for a Winkler bedding of contact stiffness  $k_w=180$  kN/m in contact with a road profile of roughness  $x_{\text{rms}}^r=2.5$  mm. The diagonal elements, shown by the dashed line, have a constant value slightly smaller than  $x_{\text{rms}}^r$ . This suggests that the each spring in the contact patch is almost always in contact with the road. The elements along the ‘‘secondary diagonal’’ however, show a parabolic shape. It seems that the nonlinearity in this situation causes a slow decay with the distance from the main diagonal. Fig. 6(b) shows the average (with frequency) of the time delay of the excitation matrix  $\mathbf{S}_{dd}^{\text{nl}}$ . The time delay is again linearly increasing with the distance between points and is hardly changed from the linear case. This agrees with the physical interpretation of the delayed profiles.

The nonlinearity due to the road/tyre contact relates  $\mathbf{S}_{dd}^{\text{nl}}$  and  $\mathbf{S}_{dd}^{\text{lin}}$ . If the road profile is supposed to be characterised only by its root mean square,  $x_{\text{rms}}^r$ , and the contact by its stiffness,  $k_w$ , the nonlinear tyre excitation,  $\mathbf{S}_{dd}^{\text{nl}}$ , could be expressed as a function only of these two quantities. Hence, the characterisation of this dependence of the excitation matrix with the road roughness,  $x_{\text{rms}}^r$ , and with the contact stiffness,  $k_w$ , is now taken into account. The objective is to get an estimate of the shape of the excitation rms matrix  $\mathbf{R}^{\text{nl}}$  as a function of road roughness and contact stiffness.

In fact, it is supposed that the matrix  $\mathbf{R}^{\text{nl}}$ , combined with the phase shifts in Eq. (3), contains all the information necessary to describe the excitation  $\mathbf{S}_{dd}$ . In other words, it has been supposed that the nonlinearity does not cause any change in the phase of the elements of the matrix but modifies the magnitudes. This modified excitation matrix can then be used to excite a purely linear tyre model to approximate the effects of the contact nonlinearities, in an approach that may be termed quasi-linear.

$\mathbf{R}^{\text{nl}}$  has been numerically computed for several values of the parameters  $x_{\text{rms}}^r$  and  $k_w$ , the road stiffness ranging from 30 kN/m to 300 GN/m and the road rms from 0.05 to 10 mm. Such large ranges have been chosen in order to better understand the influence of the two variables on the matrix  $\mathbf{S}_{dd}^{\text{nl}}$ , although the value at the ends of these ranges are unrealistic. In fact, values around 180 kN/m for the contact stiffness seem to be the most realistic [13, 14].

Fig. 7 shows the results of the mean value of the main diagonal of the rms of the excitation matrix,  $E(\text{diag}(\mathbf{R}^{\text{nl}}))$ , for different values of contact stiffness  $k_w$  and road roughness  $x_{\text{rms}}^r$ . For low contact stiffnesses the average value along the diagonal is almost equal to  $x_{\text{rms}}^r$ , meaning that along the contact patch most of the springs are always in contact with the ground. This situation can be referred as one of weak non linearity since it causes small change in the excitation matrix. As will shown in the next section, the shape of the excitation matrix in this region varies only with  $x_{\text{rms}}^r$  and is constant with  $k_w$ . For greater stiffnesses, Fig. 7 shows that for each  $x_{\text{rms}}^r$  there is a threshold contact stiffness above which  $E(\text{diag}(\mathbf{R}^{\text{nl}}))$  starts decreasing and the effect of the nonlinearity is stronger as fewer and fewer springs are in contact with the road. The weak nonlinearity threshold decreases with  $x_{\text{rms}}^r$ , so that is possible to draw approximately a threshold line (see green dashed line in the figure). The interaction between the tyre and road is thus weakly nonlinear for the most realistic contact stiffnesses at all road roughnesses below about 5 mm rms.

Supplementary tests have also been carried out to investigate the influence of a regular longitudinal tread on the nonlinear excitation matrix. The results showed that in order to take into properly account for the discontinuities due to tread, the lateral distortion of the contact elements should be taken into account, a complication that will not be discussed here.

## 4 Linearity range and approximated tyre excitation matrix

The non linear excitation matrix,  $\mathbf{S}_{dd}^{\text{nl}}$ , could be predicted from an approximation of the rms excitation matrix  $\mathbf{R}^{\text{nl}}$ , in order to avoid calculating the excitation from a time-domain nonlinear analysis. The validity of this approximation has been investigated for contact stiffness up to 300 kN/m, since greater contact stiffnesses are not considered realistic. In this stiffness range the nonlinearity is weak and the approximation is straightforward. In fact in this stiffness range the diagonal of  $\mathbf{S}_{dd}^{\text{nl}}$  could be approximated with a constant value equal to  $x_{\text{rms}}^r$ . On the other hand, the values along the secondary diagonal tend to roll down proportionally to the distance between contact points.

In order to find an approximated rms excitation matrix,  $\mathbf{R}^{\text{fit}}$ , the secondary diagonal of  $\mathbf{R}^{\text{nl}}$  has been fitted with a second order polynomial curve, which was found to fit the changes observed in the nonlinear simulations reasonably well. The elements in the matrix have been addressed by their position in the contact patch. In particular  $x_d$  has been posed as the principal diagonal reference system, with the origin in the middle of the diagonal, that is in the middle of the contact patch and,  $y_d$  has been posed as the secondary diagonal reference system. A three dimensional polynomial curve with one unknown parameter,  $c_f$ , has then been chosen:

$$r^{\text{fit}}(x_d, y_d) = x_{\text{rms}}^r + c_f y_d^2 \quad (6)$$

where  $r^{\text{fit}}(x_d, y_d)$  is the value of the element of the matrix  $\mathbf{R}^{\text{fit}}$  located at  $(x_d, y_d)$ . The parameter  $c_f$  represents the curvature of the excitation rms matrix along the secondary diagonal. This can then be used as an indicator of the linearity range.

The function in Eq. (6) has been fitted to the  $\mathbf{R}^{\text{nl}}$  matrices generated by the simulations for different values of  $k_w$  and  $x_{\text{rms}}^r$ . The constant  $c_f$  of Eq. (6) can then be found as function of the bedding stiffness and road roughness. Fig. 8 shows how the constant  $c_f$  fitted from these results varies linearly with  $x_{\text{rms}}^r$  but does not depend greatly on the contact stiffness. This supports the decision to call this region weakly nonlinear. A line,  $c_f = m_f x_{\text{rms}}^r$ , can be fitted to this data so to obtain:

$$r^{\text{fit}}(x_d, y_d) = x_{\text{rms}}^r (1 + m_f y_d^2) \quad (7)$$

where  $m_f$  is a constant equal to  $-14.7 \text{ m}^{-2}$  if  $x_{\text{rms}}^r$ .

From the approximated rms excitation matrix  $\mathbf{R}^{\text{fit}}$ , it is then possible to find an approximated excitation matrix to be used in a linear tyre model. This will improve the results that can be obtained with an excitation matrix derived from the linear model, without the complications and computational expense of a full nonlinear analysis. The approximated excitation matrix  $\mathbf{S}_{dd}^{\text{fit}}$  can be found from  $\mathbf{R}^{\text{fit}}$  supposing that the contact nonlinearity does not cause any

change in the phase value of the matrix or to the shape of the spectrum. With such a supposition the approximated excitation matrix,  $\mathbf{S}_{dd}^{\text{fit}}$ , can be written as

$$\mathbf{S}_{dd}^{\text{fit}} = \mathbf{S}_{dd}^{\text{lin}} \odot \left( \frac{\mathbf{R}^{\text{fit}}}{x_{\text{rms}}^r} \right)^2 \quad (8)$$

where  $\odot$  is the element-wise product [15], and  $\mathbf{S}_{dd}^{\text{lin}}$  is a single matrix of power and cross spectral densities, as defined in Eq. (3).

## 5 Validation on a 2D linear model

The different excitation matrices (linear, nonlinear and approximated) can be applied to the linear stochastic ring model of the tyre dynamics to compute its response [3]. The linear model used here is an elemental tyre model, connected to the ground by a Winkler contact bedding, that is assumed to be always in contact with the road. The vector of complex radial velocities of the tyre elements,  $\mathbf{v}_T$ , are assumed to be related to the vector of road displacement  $\mathbf{d}$ , via the matrix of structural mobilities,  $\mathbf{T}$ , so that [3]

$$\mathbf{v}_T = \mathbf{T}\mathbf{d} \quad (9)$$

The spectral density matrix of the tyre's velocities can be defined as

$$\mathbf{S}_{vv} = \text{E} [\mathbf{v}_T \mathbf{v}_T^{\text{H}}] \quad (10)$$

Given Eq. (9) and since the tyre model is a continuous linear systems subject to stationary random excitation,  $\mathbf{S}_{vv}$  may be expressed in terms of the spectral density matrix of road displacements,  $\mathbf{S}_{dd}$ , as

$$\mathbf{S}_{vv} = \mathbf{T}\mathbf{S}_{dd}\mathbf{T}^{\text{H}} \quad (11)$$

The expectation of the kinetic energy,  $U_{\text{ke}}$ , can be calculated considering the mass normalised mode shape matrix,  $\mathbf{\Psi}$ , and it is given by

$$U_{\text{ke}}(\omega) = \frac{1}{2} \text{trace} \{ \mathbf{\Psi}^+ \mathbf{S}_{vv} \mathbf{\Psi}^{+\text{H}} \} \quad (12)$$

where  $(\cdot)^+$  is the pseudo-inverse operator.

The excitation matrices  $\mathbf{S}_{dd}^{\text{lin}}$ ,  $\mathbf{S}_{dd}^{\text{nl}}$  and  $\mathbf{S}_{dd}^{\text{fit}}$  have then been applied to the 2D linear model with the parameters given in [3], to evaluate the accuracy of the quasi-linear approximation on the predicted tyre vibration.  $\mathbf{S}_{dd}^{\text{lin}}$  is the linear excitation matrix and is given by Eq. (3).  $\mathbf{S}_{dd}^{\text{nl}}$  is the non linear excitation matrix and is obtained by calculating the auto and cross-spectra of the spring displacements from the full nonlinear model.  $\mathbf{S}_{dd}^{\text{fit}}$  is an approximated matrix obtained, as in Eq. (8), from the rms approximated matrix  $\mathbf{R}^{\text{fit}}$ , which in turn is found from the constant  $c_f$  of Eq. (6).

The tyre vibration and its kinetic energy have been obtained for different excitation matrices by substituting  $\mathbf{S}_{dd}^{\text{lin}}$ ,  $\mathbf{S}_{dd}^{\text{nl}}$  or  $\mathbf{S}_{dd}^{\text{fit}}$ , into Eq. (11). Fig. 9(a) shows the kinetic energy of the tyre model under these three conditions ( $U_{\text{ke}}^{\text{lin}}$ ,  $U_{\text{ke}}^{\text{nl}}$  and  $U_{\text{ke}}^{\text{fit}}$ ) when  $k_w=180$  kN/m,  $x_{\text{rms}}^r=2.5$  mm and  $v=40$  km/h. The difference between  $U_{\text{ke}}^{\text{lin}}$  and  $U_{\text{ke}}^{\text{nl}}$  in Fig. 9(a) is not great, supporting the supposition that we are dealing with a weak nonlinearity. The difference is most noticeable at around 100 Hz, that is in correspondence of the intersection of the two split lines ( $f_2 = cn_2 \approx 110$  Hz). For frequencies from about 20 to 60 Hz  $U_{\text{ke}}^{\text{nl}}$  is slightly greater than  $U_{\text{ke}}^{\text{lin}}$  while for high frequency  $U_{\text{ke}}^{\text{nl}}$  is slightly lower than  $U_{\text{ke}}^{\text{lin}}$ . The behaviour at high frequencies can be explained by the fact that less points are in contact, and so the auto-spectra of the excitation are slightly lower. The behaviour of the nonlinear system at low frequency may be due to the fact that the excitation signal are flattened, increasing the relative level of the low frequency energies of the signal, as seen in Fig. 1.  $U_{\text{ke}}^{\text{fit}}$  follows the behaviour of the nonlinear simulation around 110 Hz quite well, which is the range in which the nonlinearity is most evident. In the frequency range, however,  $U_{\text{ke}}^{\text{fit}}$  follows more accurately the linear simulation result. The difference between the nonlinear and approximated nonlinear excitation is particularly evident for frequency lower than 60 Hz, where the calculated spectral densities will be subject to the greatest estimation error.

Fig. 9(b) shows the rms velocity distribution of the elements around the tyre, computed by integrating the individual spectra for the elements between 60 and 1000 Hz, thus excluding the unreliable low frequencies results. The centre of the contact area is at zero degree. Difference between linear, nonlinear and approximated nonlinear simulations are small, but the fitted results lie between the linear and nonlinear results and are generally closer to the nonlinear results. It should also be observed, however, that the results from the linear model are not a bad approximation to those from the full, nonlinear, analysis for this weakly nonlinear case, which appears to be typical of normal conditions.

## 6 Conclusions

The displacement of a tyre when in contact with the road has been calculated by applying a nonlinear contact algorithm to a Winkler bedding. The spectral density distributions for the tyre excitation from linear and nonlinear analyses have been investigated. It has been shown that, when the contact stiffness is sufficiently low but still realistic, the nonlinearity change the shape of the excitation matrix mainly along the secondary diagonal. It has also shown that the curvature of the secondary diagonal in this weakly nonlinear range depends mainly on the road roughness.

A modified excitation matrix for use in a fully linear stochastic road/tyre model has then been proposed. Such an approximation appears valid for realistic contact value and depends only on the road roughness. The validity

of such an approximations has been tested numerically on a 2D tyre model. The approximated excitation gives a good approximation of the nonlinear excitation for the computation of the tyre kinetic energy above 60 Hz. However such an approximation still underestimates the velocity of the tyre below 60 Hz compared with the nonlinear simulations.

## 7 Figures

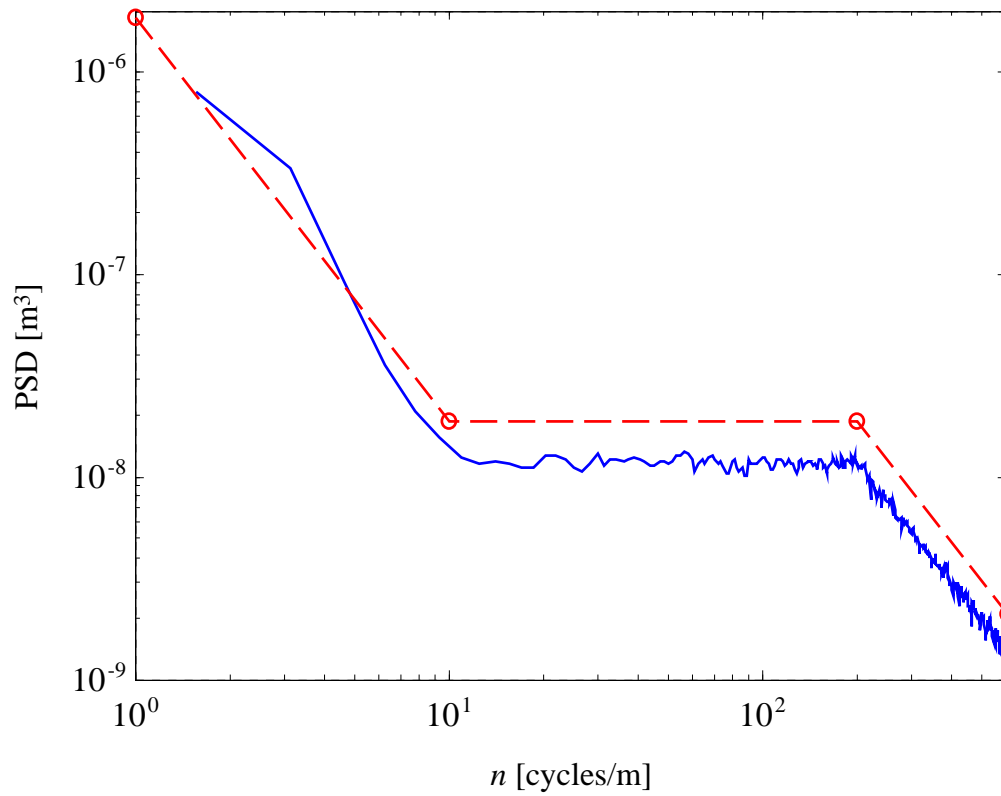


Figure 1: Piecewise linear approximation of the PSD of a common road profile (red dotted line). PSD of the generated road profile used in the time-domain nonlinear simulations (continuous blue line).

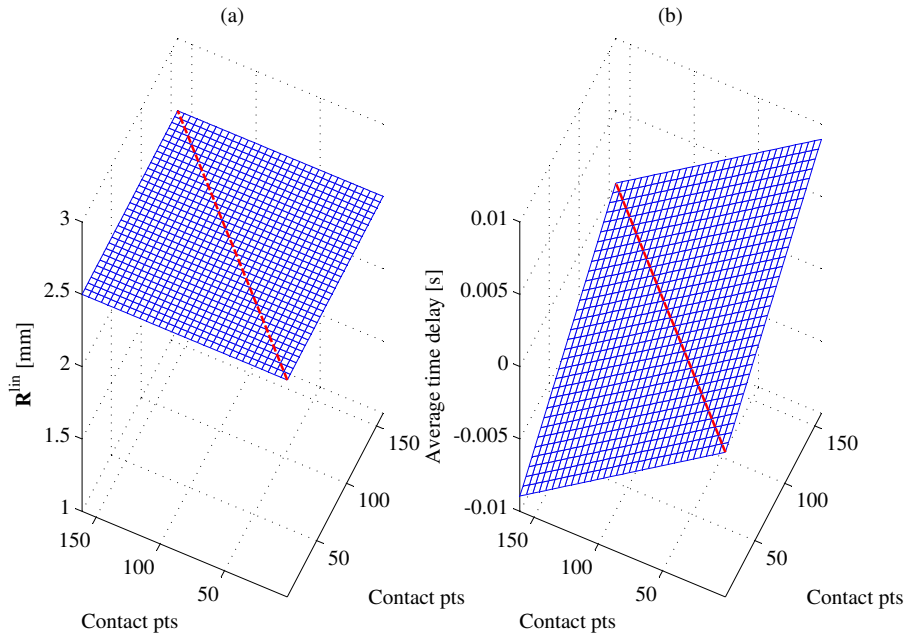


Figure 2: Representation across the contact patch of  $\mathbf{R}^{\text{lin}}$  (a) and average  $\mathbf{S}_{dd}^{\text{lin}}$  time delay (b) calculated from the linear model for  $x_{\text{rms}}^r = 2.5$  mm and  $v = 40$  km/h. The main diagonal element are shown as dashed line.

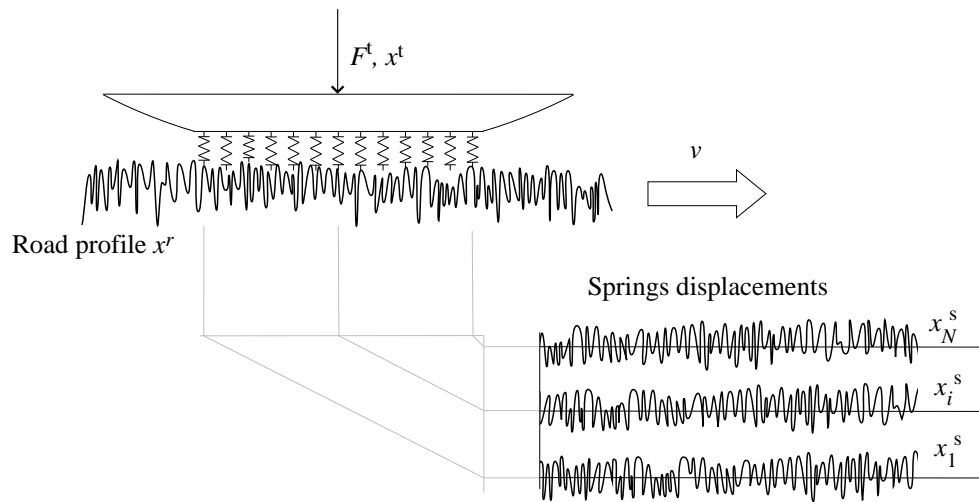


Figure 3: Schematic representation of the nonlinear contact algorithm.  $x^r$  road profile;  $F^t$  static force acting on the tyre;  $x^t$  displacement of the tyre;  $x_i^s$  ( $i = 1, \dots, N_c$ ) displacements of the  $N_c$  spring in the contact patch.

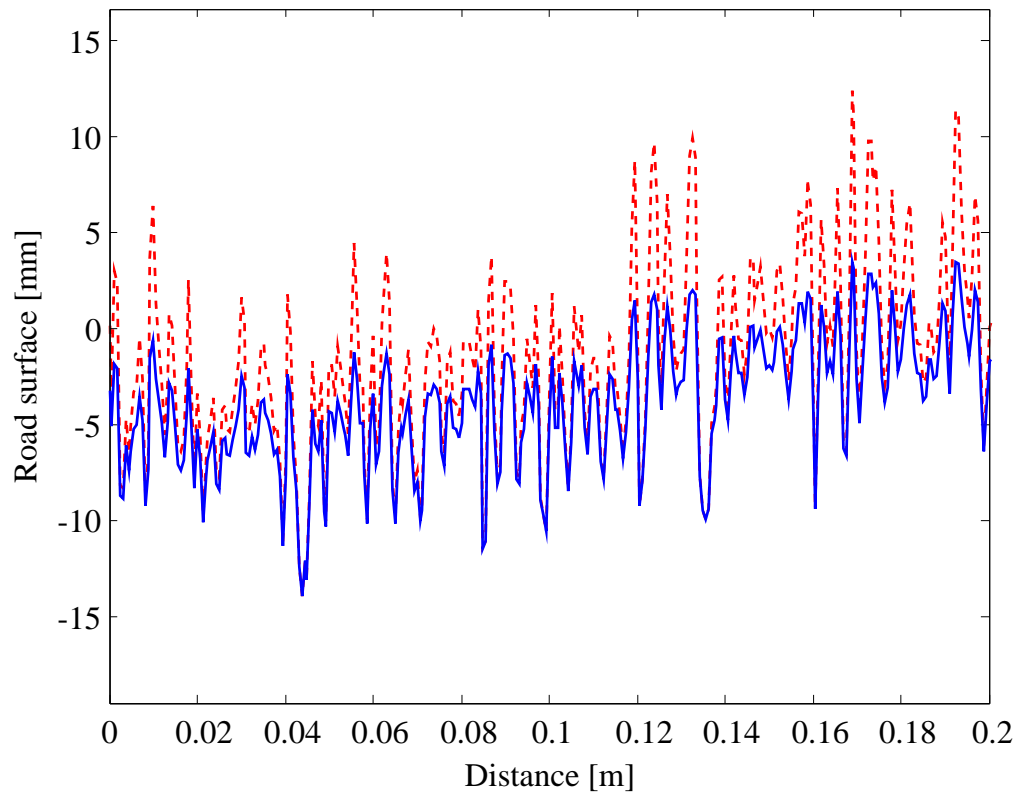


Figure 4: Road profile before (dotted red line) and after (continuous blue line) the application of the nonlinear transformation to flatten the peaks on the road profile.

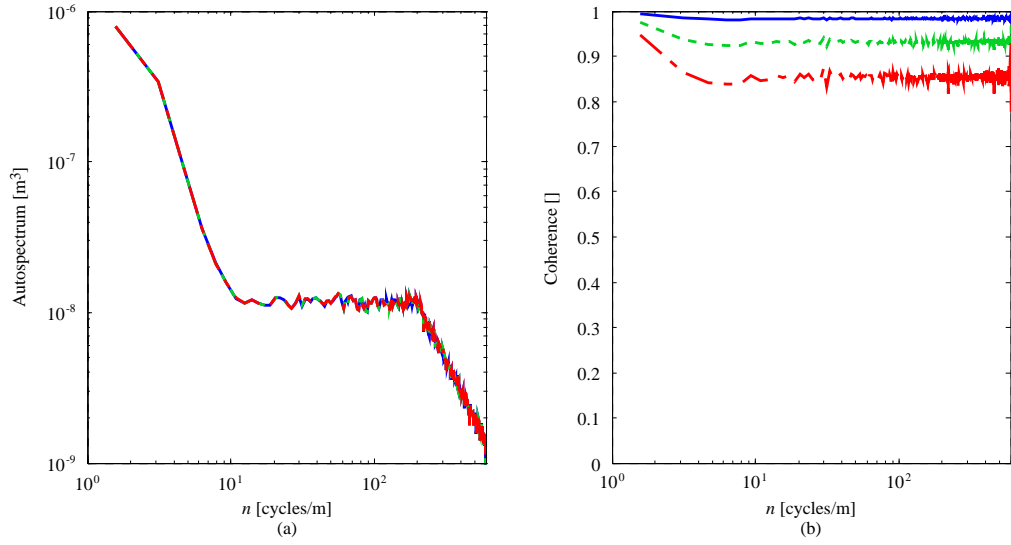


Figure 5: (a) Spectra of the nonlinear excitation spectral matrix ( $x_{\text{rms}}^r=2.5$  mm,  $k_w=180$  kN/m): the continuous blue line refers to a point at the edge of the contact patch, the dot-dash red line to the point in the centre of the contact patch and the dashed green line to the point between these two. (b) Coherences between the nonlinear contact displacements ( $x_{\text{rms}}^r=2.5$  mm,  $k_w=180$  kN/m): the continuous blue line represents the coherence between two points 23 mm apart, the dashed green line to points 47 mm apart and the dot-dash red line to points 70 mm apart.

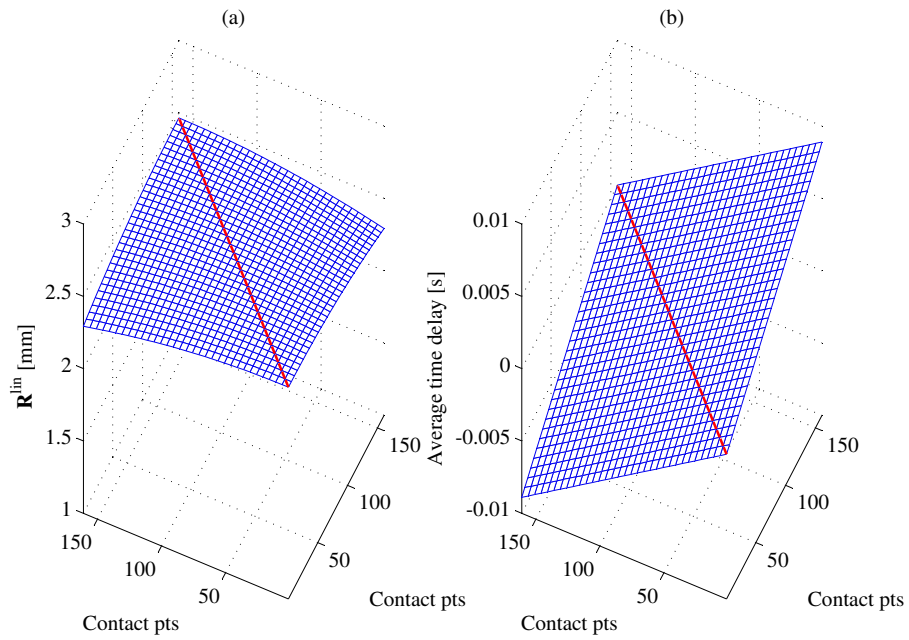


Figure 6: Representation across the contact patch of  $\mathbf{R}^{\text{nl}}$  (a) and average  $\mathbf{S}_{dd}^{\text{nl}}$  time delay (b) calculated from the linear model for  $x_{\text{rms}}^{\text{r}}=2.5$  mm and  $v=40$  km/h.

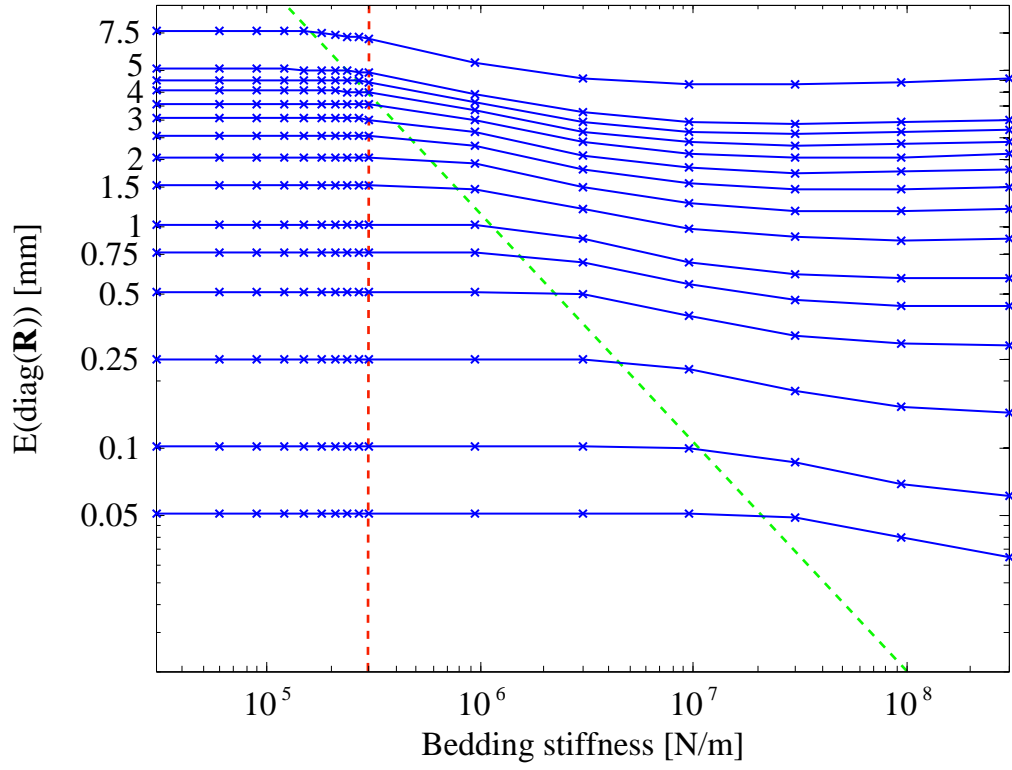


Figure 7: Change of the mean value of the diagonal of the matrix  $\mathbf{R}^{\text{nl}}$  with the bedding stiffness  $k_w$  for various road profiles rms  $x_{\text{rms}}^r$  calculated from the results of many nonlinear simulations. The green dashed line indicate approximately the weak nonlinearity threshold. The dashed red line indicate the maximum stiffness of interest here which is about 300 kN/m.

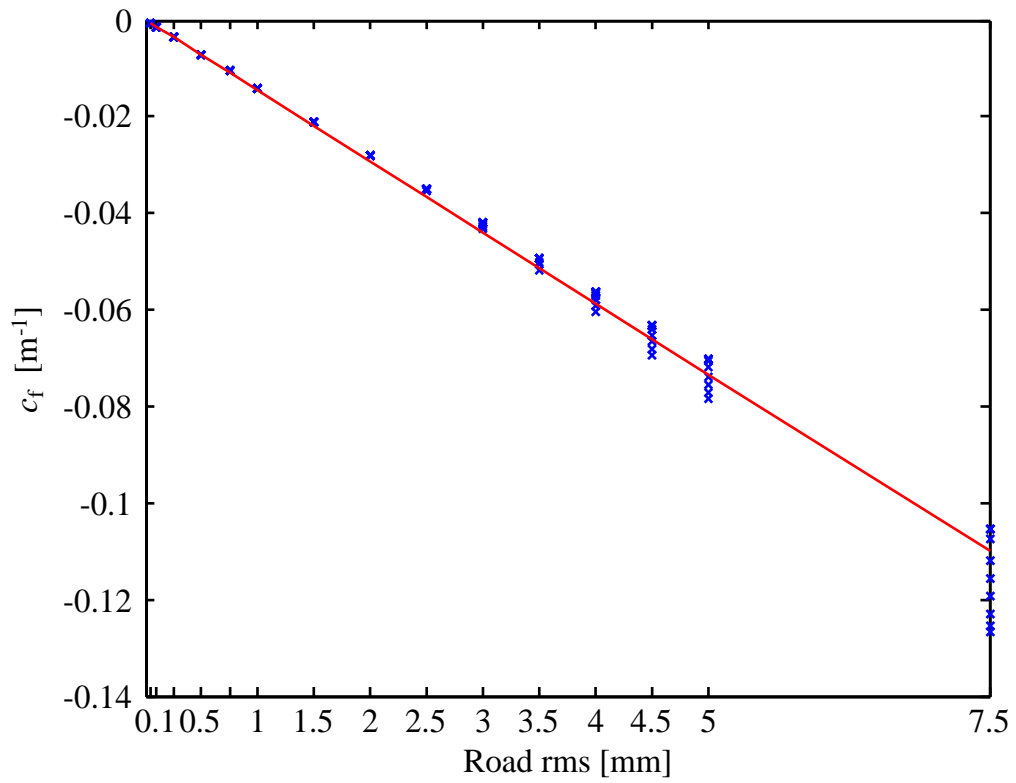


Figure 8: Variation of fitted value of the parameter  $c_f$  in Equation (6) with the road roughness  $x_{\text{rms}}^r$ . The blue points show computed points for different contact stiffnesses  $k_w$ . The red line is a linear fit of the points.

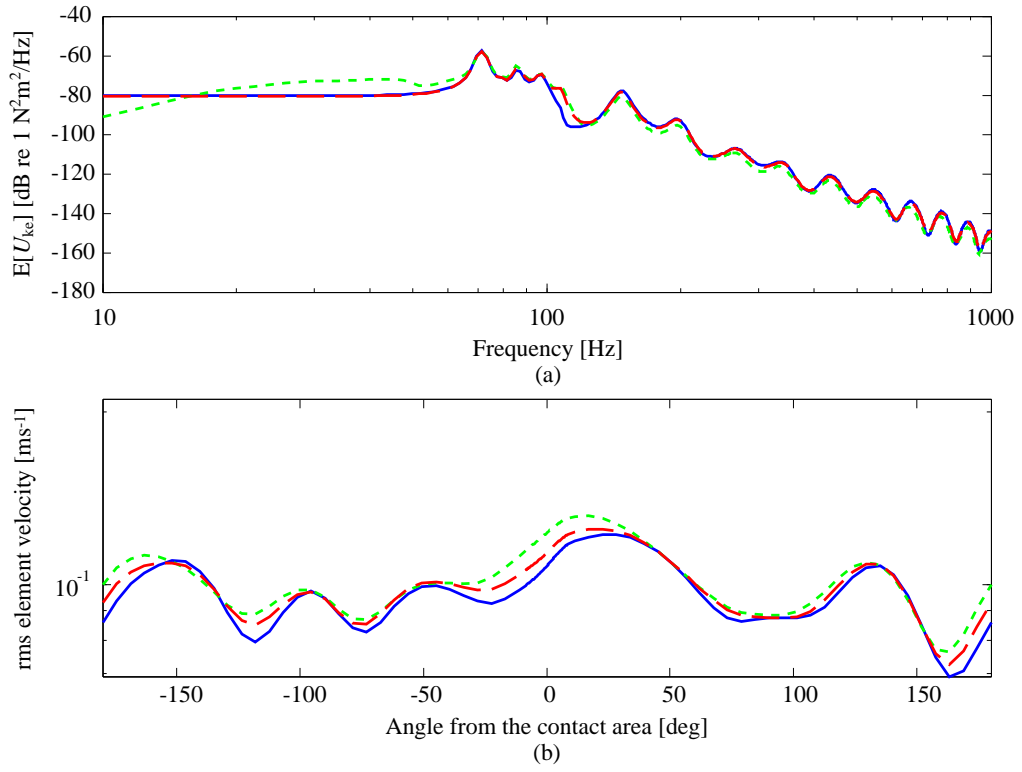


Figure 9: Average kinetic energy spectrum (a) and rms velocity around the tyre (b) for  $x_{\text{rms}}^r=2.5$  mm,  $k_w=180$  kN/m and  $v=40$  km/h. Continuous blue line refers to linear excitation matrix; dotted green line refers to nonlinear excitation matrix; dashed red line refers to approximated nonlinear excitation matrix.

## References

- [1] U. Sandberg, G. Descornet, Road surface influence on tyre/road noise, in: *Inter-noise*, Vol. 1, Miami, Florida, USA, 1980, pp. 259–272.
- [2] S. Fong, Tyre induced predictions from computed road surface texture induced contact pressure, in: *Inter-noise*, Christchurch New Zealand, 1998.
- [3] E. Rustighi, S. J. Elliott, Stochastic road excitation and control feasibility in a 2d linear tyre model, *Journal of Sound and Vibration* 300 (3-5) (2007) 490–501.
- [4] K. L. Johnson, *Contact mechanics*, Cambridge University Press, 1985.
- [5] P. André, Power spectral density approximations of longitudinal road profiles, *International Journal of Vehicle Design* 40 (1/2/3) (2006) 2–14.
- [6] C. J. Dodds, J. D. Robson, The description of road surface roughness, *Journal of Sound and Vibration* 31 (2) (1973) 175–183.
- [7] M. Sayers, Characteristic power spectral density function for vertical and roll components of road roughness, in: L. Segel, J. Y. Wong, E. H. Law, D. Hrovat (Eds.), *Symposium on Simulation and Control of Ground Vehicles and Transportation Systems*, Vol. AMD-80, DSC-2, The American Society of Mechanical Engineering, Anaheim, CA, 1986, pp. 113–129.
- [8] J. Robson, Road surface description and vehicle response, *Int. J. of Vehicle Design* 1 (1) (1979) 25–35.
- [9] D. E. Newland, *An introduction to random vibrations, spectral & wavelet analysis*, 3rd Edition, Dover Publications, Inc., 1993.
- [10] J. Périssé, A study of radial vibrations of a rolling tyre for tyre-road noise characterisation, *Mechanical Systems and Signal Processing* 16 (6) (2002) 1043–1058.
- [11] R. Pinnington, Personal communication (September 2007).
- [12] U. Sandberg, J. A. Ejsmont, *Tyre/road noise reference book*, Informex Ejsmont & Sandberg Handelsbolag, 2002.
- [13] K. Larsson, *Modelling of dynamic contact - exemplified on the tyre/road interaction*, Ph.D. thesis, Department of Applied Acoustics, Chalmers University of Technology, Göteborg, Sweden (2002).
- [14] G. Gäbel, M. Kröger, Non-linear contact stiffness in tyre-road interaction, in: *Euronoise 2006*, Tampere, Finland, 2006, paper 118.

- [15] H. Lütkepoh, Handbook of Matrices, John Wiley & Sons, Inc., New York, 1996.